AD-A142 192 A-O EXCISOR(U) WESTINGHOUSE DEFENSE AND ELECTRONICS 1/1
CENTER BALTIMORE MD ADVANCED TECHNOLOGY DIV
G M BORSUK ET AL. NOV 79 N00039-79-C-0127

UNCLASSIFIED F/G 9/5 NL

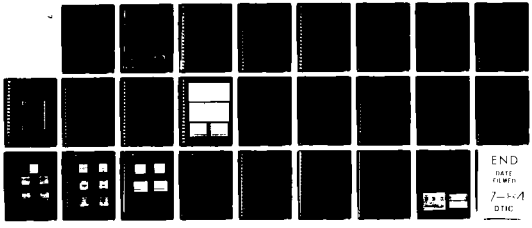

END
DATE FILMED
7-84
DTIC

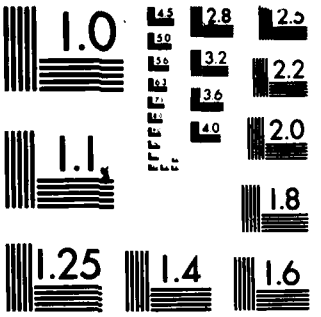

AD-A142 192

DTIC FILE COPY

2

A-O EXCISOR

FINAL REPORT

NAVALEX Contract No. N00039-79-C-0127

Submitted to:

NAVAL ELECTRONIC SYSTEMS COMMAND

WASHINGTON, D. C. 20360

NOV 1979

BY:

G. M. BORSUK, F. KUB, M. RANDOLPH

WESTINGHOUSE ELECTRIC CORPORATION

ADVANCED TECHNOLOGY DIVISION

P. O. BOX 1521, M. S. 3531,

BALTIMORE, MARYLAND 21203

A-O EXCISOR

FINAL REPORT

1.0 INTRODUCTION

A 100 element silicon integrated circuit photosensor array has been developed that when used with a coherent A-O processor allows the real-time excision of narrow band interferers (1MHz) over a large instantaneous bandwidth (100MHz). The fundamental operations necessary to perform this task are the transformation of the signal to the frequency domain (retaining both amplitude and phase), point-by-point multiplication by a prescribed excision function, H(f), and transformation back into the time domain.

The combined system of the sensor array, which provides the excision function and conversion to the time domain, and the coherent A-O processor, which Fourier transforms the signal from the time domain to the frequency domain, provides the function of a programmable notch filter. Two designs of the photosensor excisor have been built and tested. They are both contained on the 5066 mask set. The more conventional design consists of a linear array of 100 photodiodes connected to two output buses through a bank of MOS transistor switches. In the second design, the photodetector's output signals are steered to the preselected summing bus by electric field switches which have a wideband frequency response. The wideband frequency response

is possible even though the signal currents maybe very small ($\approx 10^{-6}$amps). The excisor chips have been extensively tested and used in several coherent A-O signal processing systems. Two papers are included in the Appendix. The first paper details the use of the device in an A-O signal processor configured as a sub-band filter while the second paper describes its uses as a 100-point programmable correlator.

2.0 TECHNICAL DISCUSSION

The 100 element photosensor device is intended for use with an A-O signal processor to form a programmable electrical notch filter system. A block diagram of the photosensor architecture is shown in Figure 1, and of the coherent A-O system in Figure 2. A description of the A-O processor is given below. A laser beam is passed through an A-O Bragg cell which splits the incident laser beam into deflected and undeflected components. The deflected beams are caused by the moving volume phase grating formed by acoustic waves launched in the Bragg cell by the RF driven transducers. These acoustic waves modulate the A-O cell's index of refraction in time and space. The modulation produces deflected optical beams which for our purpose are spatially resolved and correspond to the RF signals applied to the Bragg device. This operation corresponds to an instantaneous Fourier transform of the applied RF signal. In addition to the frequency to spatial transform, each spatially resolved optical beam is doppler shifted in frequency corresponding to the applied RF signal. Thus, the resolved optical beam will have frequency components given by $(\nu_o + \nu^*)$ or $(\nu_o - \nu^*)$ where ν^* is the applied RF signal and ν_o is the optical frequency. The direction of the acoustic wave in relation to the

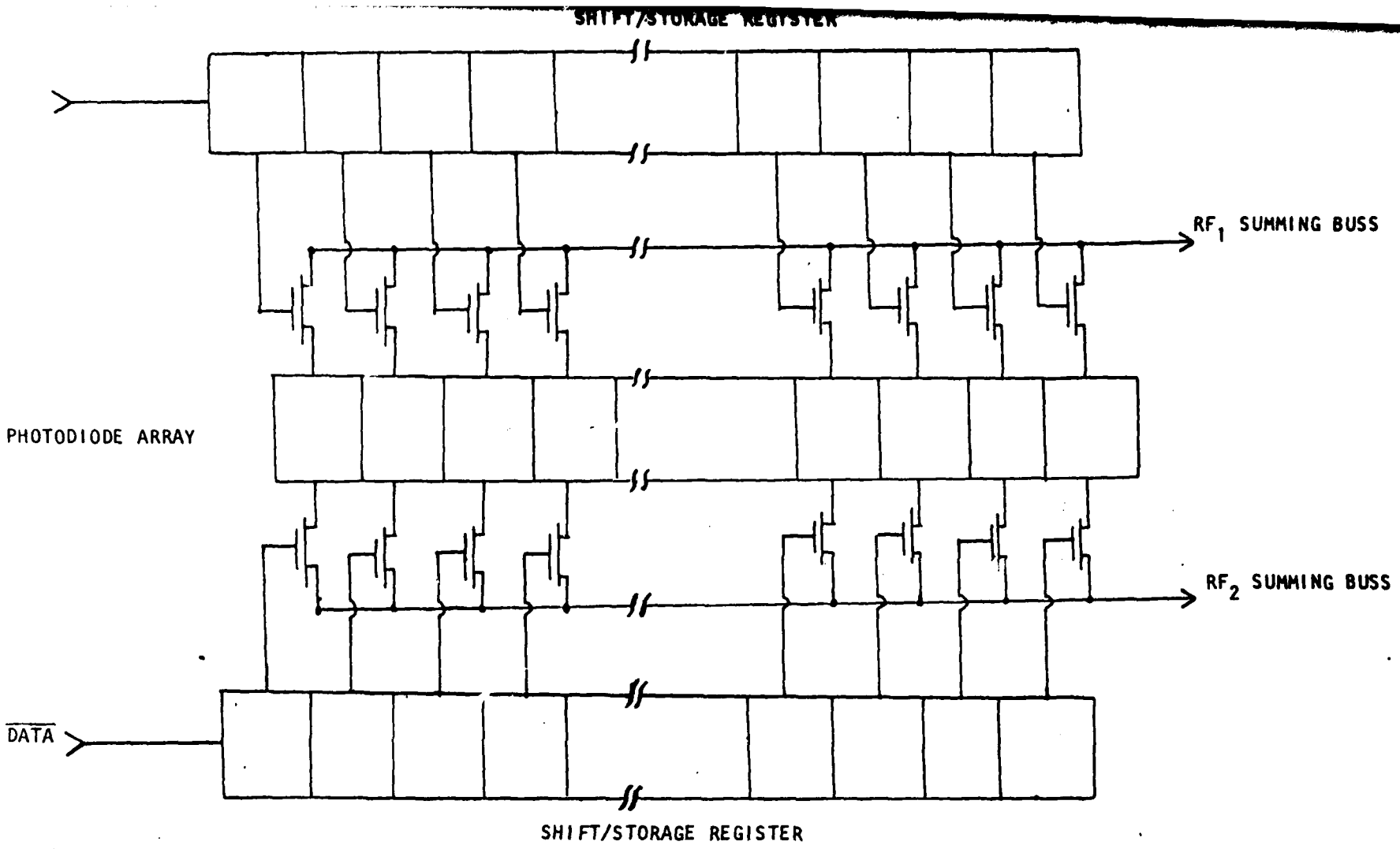

FIGURE 1 - A-O EXCISOR DETECTOR

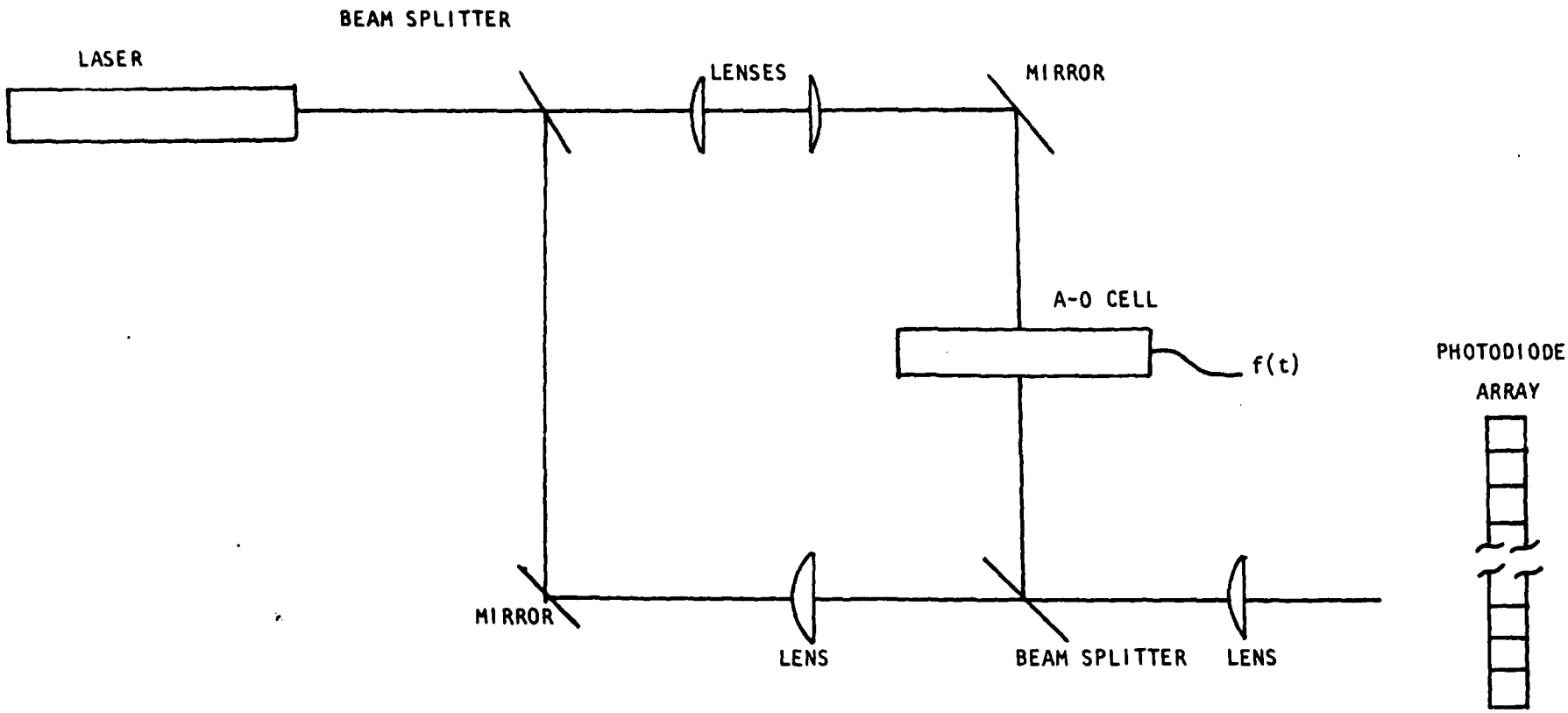

FIGURE 2 - INTERFEROMETRIC SPECTRUM ANALYZER

optical beam determines whether the diffracted optical beam is doppler up-shifted or down-shifted. The undeflected laser beam of frequency ν_o is also imaged upon the photosensor array as shown in Figure 2.

Since the laser is a coherent source of optical energy (within a given path length), the superposition of the zero order and diffracted laser wavefronts reaching the array produce optical mixing. The mixing operation occurs because the photosensors are square law detectors. The intensity profile is proportional to the square of the summed wavefront amplitudes. The resultant intensity in a resolved spot will contain frequency products of ν_o, and the doppler shifted frequency $(\nu_o + \nu^*)$ amd $(\nu_o - \nu^*)$. The result from the mixing operation is a component at $2\nu_o + \nu^*$ (or $2\nu_o - \nu^*$)and ν^*. Since the lasers optical frequency is around 10^{14} Hertz, much above the passband of the sensor, the sensor will only respond to the lower doppler shift frequency beat note located within the RF band. Each pixel of the sensor, occupying a different spatial location, will receive different RF frequencies. However, each pixel must have a sufficient frequency response to accommodate the beat note frequency present in the mixed optical signal intensity. A detailed theory of optical heterodyning is presented in Appendix A. The mean-square beat signal power resulting at the load resistor is:

$$S = 2 I_1 I_2 R_L$$

where I_1 is the signal photocurrent and I_2 is the zero order pump

photocurrent. Since I_2 is usually much larger than I_1 the system response is linearized. The power gain, comparing the case of optical heterodyning to direct detection,

$$G=2I_2/I_1$$

For small signal powers this gain can be in the range of 10^5 to 10^6.

The photosensor architecture, shown in Figure 1, along with the coherent A-O processes described above implements a programmable notch filter. As shown in Figure 2, each photosensor element has two switches that connect the photosensor to either summing buss RF_1 or RF_2. The state of the switch is controlled by the DATA pattern stored in static shift registers that are located on either side of the photosensor array. Complimentary data patterns are stored in the two shift registers so that in each pair of switches connecting the photodiode to the output summing busses, one switch is ON and the other is OFF. The use of complimentary signals to control each pair of transistor switches guarantees that each photosensor element is only connected to a single summing buss at a time.

Thus, the excision function is implemented by programming selected switches to be in the OFF state. Since each pixel of the sensor will receive different RF beat note frequencies, certain beat note frequencies can be excised. All beat note frequencies not excised will be summed together on a single output summing buss. Thus, the electrical output will be a time domain

replica of the input signal with certain frequency components excised. It is necessary that the bandwidth of the switch and bandwidths of the summing buss/input amplifier be sufficient to accommodate the highest beat note frequency.

3.0 DEVICE DESCRIPTION

3.1 PHOTODIODE/MOSFET SWITCH DETECTOR

A conventional approach for realizing the required 100 element photosensor array shown in Figure 1 is to use MOSFET transistor switches for manipulating the photogenerated signals between two summing busses. In particular, pairs of transistor switches, having their common node connected to the photodetector and the other nodes connected respectively to one of the two summing busses provides the function of switching the photocurrent between two busses. Each transistor switching pair is driven by a set of two complimentary signals generated by two 100-stage static shift registers such that in each pair only one switch is on and the remaining one is off. The use of complimentary signals to control each pair of transistor switches guarantees that each photodetector is only connected to a single summing bus at a time. The shift registers are externally programmable and are programed by design, into complimentary states with respect to each other. The shift registers are serially programmable by a 100-bit-long binary data string. During programming the output from the 100 photodetectors is indeterminate.

After the device has been programmed, it is ready for signal processing. The update time for loading the data string into the registers is approximately 2 milliseconds.

Such operating conditions reduce the need for fast shift registers; however, they do not decrease the need for high quality switches. In particular, the isolation of the switches in their off state must be very high and the frequency bandpass of the switches in their on state must be very wide. Both of these operating requirements are very demanding in view of the low level signals which are being switched. The photodetector's output photocurrent signals are generally less than luA for ac and dc signals combined. The ac component of the photodetectors output signal will have frequency terms between 10 MHz and 200 MHz. These signal characteristics coupled with the small space (33um) allowed for these switches requires careful design of the switching device.

3.2 DRIFT FIELD SWITCH DETECTOR

A photodetector structure that may allow higher photosignal bandwidths than the MOSFET switch approach is shown in Figure 3. Two summing busses, labeled $\Sigma+$ and $\Sigma-$, are the p+ diffusion held at the same potential and connected to the common emitter transistor amplifiers. Carrier (holes and electrons) are generated by the laser light ($h\nu$) which is incident through the optically transparent resistive poly-silicon gate and absorbed in the n-silicon semiconductor. After photogeneration, the carriers are subjected to an electric field which is determined by the bias placed across the resistive

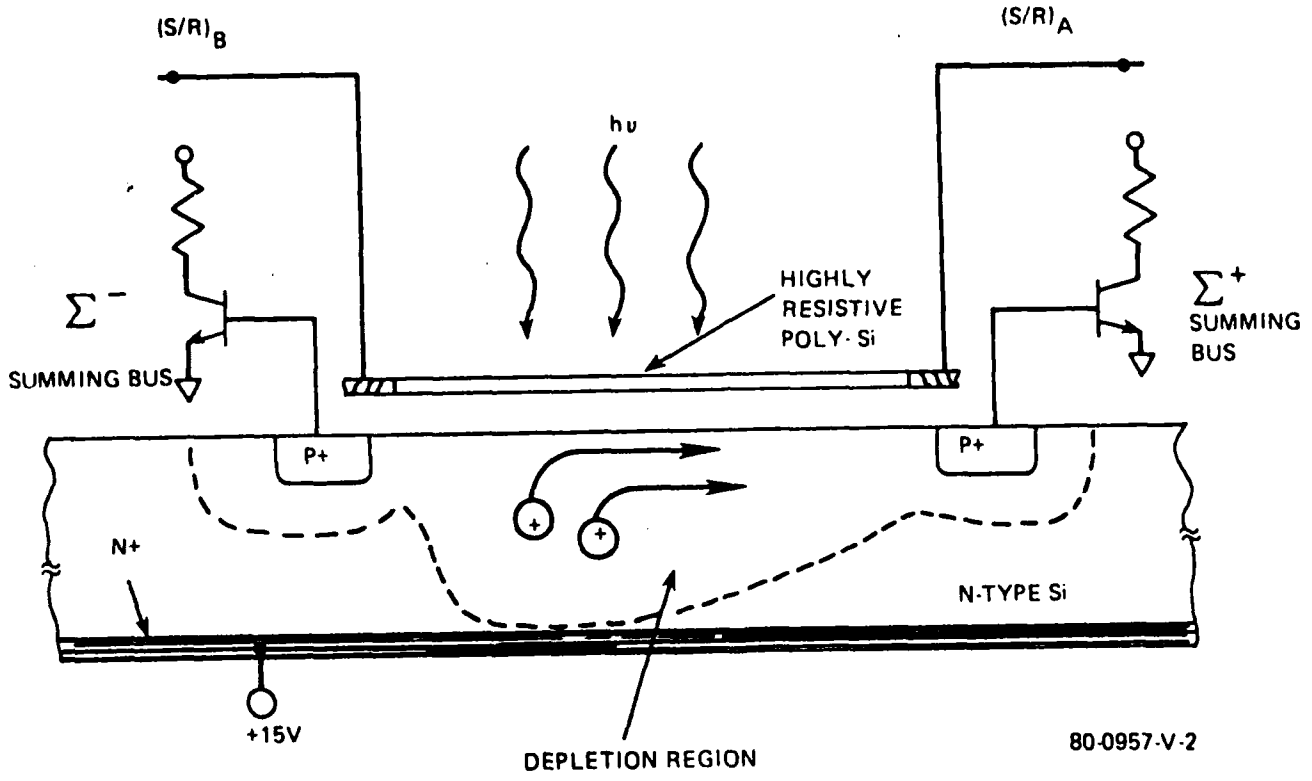

FIGURE 3 - STRUCTURE OF SWITCH EMPLOYING A DRIFT FIELD FOR STEERING PHOTOGENERATED CURRENT BETWEEN TWO SUMMING BUSSES

polysilicon gate. Sufficient bias is applied to the two summing busses and the resistive polysilicon gate to form a depletion region in the n-silicon to facilitate efficient collection of photogenerated holes by the summing busses. Photogenerated electrons are channeled in the direction of the substrate (away from the p+ summing busses) which is positively biased with +15 volts. Bias across the resistive polysilicon gate is supplied by opposing static shift register stages which are always in complimentary states relative to each other.

The electric field below the resistive polysilicon gate and in the n-type silicon region, between the two p+ summing busses has been calculated and a potential plot obtained from these calculations is shown in Figure 4. A potential placed across the polysilicon gate is such that the photogenerated holes will be collected by the left p+ diffusion in Figure 4. For the case where opposite bias is placed across the polysilicon gate the holes will be collected by the right p+ diffusion. The fields inside the depletion region will be about $5x10^3$ volts/cm. Under such conditions, the transport of photogenerated carriers to the p+ summing busses can take less than $1x10^{-9}$ seconds. Operating frequency limitations of this type of collection and field switching structure will be limited to the dispersion in the time required for photogenerated carriers to travel before they reach the the p+ busses. This time dispersion can be limited and reduced by limiting the photogeneration volume and the distance the photogenerated carriers have to travel before being collected. Limiting the operation of this detector to blue laser light should certainly reduce the time dispersion and thus further improve the frequency response of this device. Also changing the structure so that

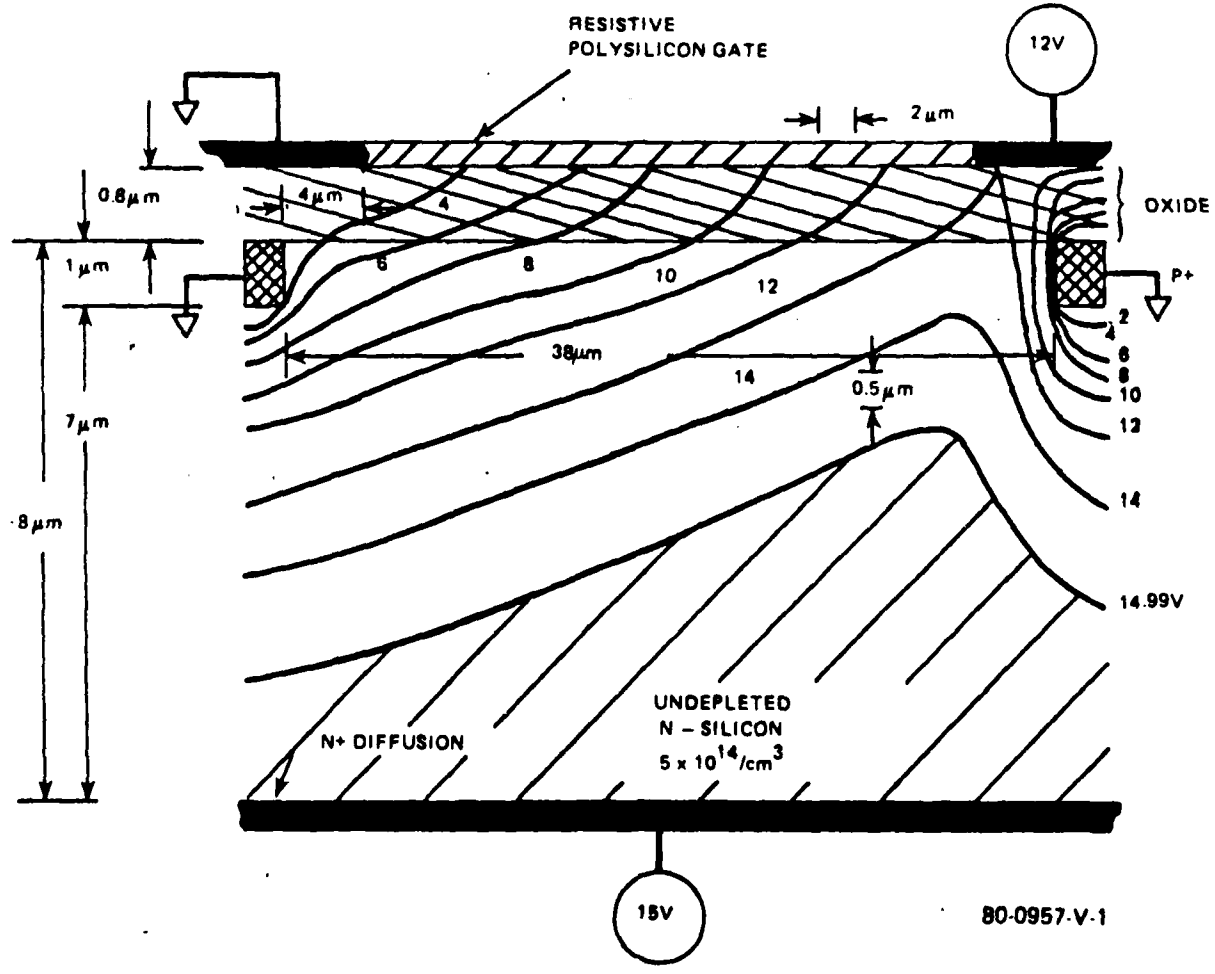

FIGURE 4 - CALCULATED POTENTIAL DIAGRAM OF STRUCTURE SHOWN IN FIGURE 3.

electrons are collected, rather than holes, will further reduce the time dispersion and improve the frequency response. The drift field switching structure is independent of current levels. The device is realized by replacing each photodiode and two transistor switches of the MOSFET switch approach by a photogeneration volume and a resistive polysilicon gate generating a drift field . All the other elements, such as shift registers and summing busses remain the same as in the case of the 100 element photosensor with transistor switches.

4.0 EXPERIMENTAL RESULTS

4.1 PHOTODIODE/MOSFET SWITCH DETECTOR

The 100-element conventional approach photodiode detector has been built and tested. Each photodiode has two MOSFET switches connected to it. The other side of the switches are connected to one of the two output summing busses. The array has been tested and was found to have a 3dB bandwidth of 125MHz with a switch-off isolation of 34dB.

The off-isolation of the MOSFET switches is a combination of two sources. One is the possibility that charge created in a given photodiode moves to an adjacent photodiode before being transferred to the power supply. The other possibility is that the MOSFET switches when turned off are not "totally" off and have capacitive feedthrough. No experiment has yet been performed to determine which is the significant component.

The limit on the bandwidth appears to be due to MOSFET switch. When the switch is on it acts like a resistor. The capacitance of the photodiode and the resistance of the MOSFET switch makes an RC low pass filter. The current design has a 3dB bandwidth both calculated and measured between 100 and 125MHz. The measured dynamic range (maximum beat note signal to noise floor) is greater than 70dB.

4.2 DRIFT FIELD DETECTORS

A 100 element photosensor device with the drift field switches has been built and tested (Figure 5). The center section of the device contains the drift field switches, (See Figure 6), which are connected to and driven by two 100-element static shift registers. A resistive polysilicon layer, rectangular in shape, is connected between two bias lines on opposite sides supplied from two static shift registers that are in complementary states. These resistive polysilicon gates are disposed adjacent to each other on a 33um pitch to form the 100-element detector. The definition of the detector's active area is limited to the polysilicon resistive gate by a light shield not shown. The 100-element line array was fabricated and tested. Results obtained are shown in Figures 7 and 8.

A single RF frequency is applied to the A-O system shown in Figure 1. This frequency of 76.9 MHz manifested itself on the side one bus when it is turned on. The amplitude of the frequency signal is -50dBm (see Figure 7). When the resistive field switch is toggled to apply the photogenerated signal to the second bus, the amplitude of the 76.9 MHz signal decreases by 24dB (see

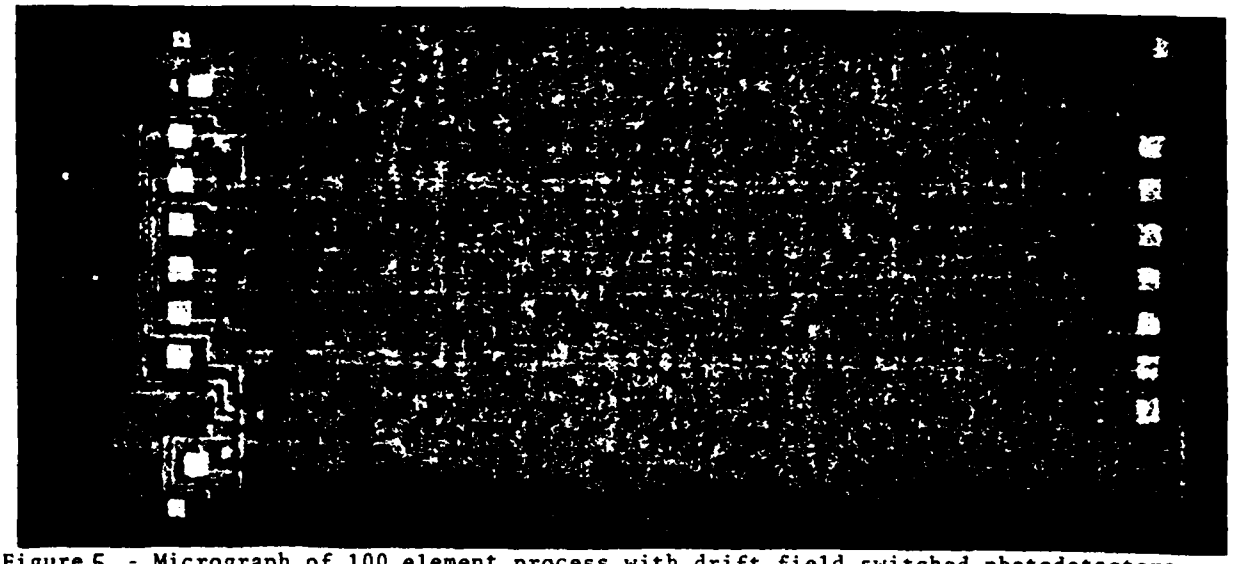

Figure 5 - Micrograph of 100 element process with drift field switched photodetectors controlled by two 100 element static shift registers.

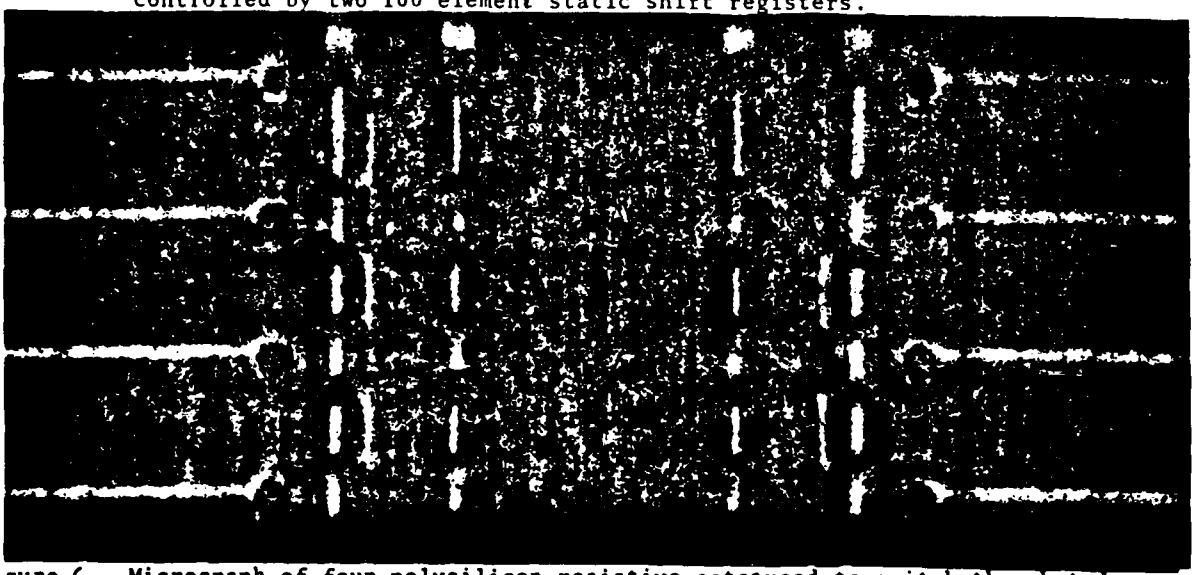

Figure 6 - Micrograph of four polysilicon resistive gates used to switch the photodetectors in the device shown in Figure 5.

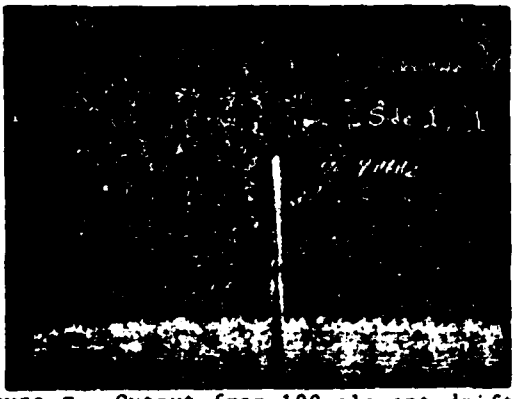

Figure 7 - Output from 100 element drift field switch processor with bus number one on.

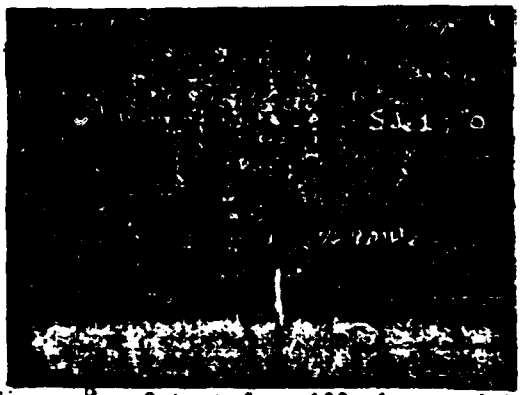

Figure 8 - Output from 100 element drift field switch processor with bus number one off.

Figure 8) on the one bus and now appears on the second bus. Some amplitude at 76.9 MHz still remains above the noise level on bus one as shown in Figure 8. The incomplete switch-over of the signal is due in part to the lack of a light shield on the device tested and electrical isolation problems with the peripheral off-chip processing circuitry.

5.0 CONCLUSIONS

Both the conventional MOSFET switch and drift field switch photosensor have been built and evaluated. The measured off-isolation of the MOSFET switch photosensor is 34dB while the measured off-isolation of the drift field switch is 24dB. The measured 3dB bandwidth of the MOSFET switch is approximately 125MHz. The bandwidth of the drift field switch has not been evaluated. The poorer isolation of the drift field switch is probably attributed to photogenerated carriers in the bulk of the detector diffusing to the off-buss P+ collector diffusion. The dynamic range of the MOSFET photosensor is greater than 70dB.

Analysis of the MOSFET switch approach indicates that both the bandwidth and off-isolation of the switch can be improved by increasing the MOSFET length to width ratio. The calculated bandwidths for improved W/L ratios is approximately 500MHz. Additional silicon processing techniques and circuit design techniques may allow an additional improvement in switch bandwidths.

There are no inherent limitations to increasing the number of detector elements beyond 100 elements except for yield considerations.

APPENDIX A

THEORY OF OPTICAL HETERODYNING

A reversed biased photodiode is a square law detector and can thus be used for photomixing. Optical heterodyning consists of illuminating a photodiode with two light fields, the signal electrical field, $E_1 \cos w_1 t$ and the pump or local oscillator electrical field, $E_2 \cos w_2 t$. If these two electric fields are impinging in parallel onto a photodiode the total electric field will be:

$$E = E_1 \cos w_1 t + E \cos w_2 t$$

The photocurrent output is then

$$I = AE^2$$

where A is a constant. Substituting the former equation into the latter yields:

$$I = AE_1^2 \cos^2 w_1 t + AE_2^2 \cos^2 w_2 t + AE_1 E_2 \cos(w_1 - w_2)t + AE_1 E_2 \cos(w_1 + w_2)t$$

Because the detector cannot follow the instantaneous intensity at optical frequencies it will respond to the average of the first, second, and fourth terms. The average values are $AE_1^2/2$, $AE_2^2/2$ and zero, respectively. However, it is assumed that the detector has a sufficient bandwidth to follow the signal at the difference frequency $w_1 - w_2$. thus

$$I = 1/2AE_1^2 + 1/2AE_2^2 + AE_1E_2 \cos(w_1 - w_2)t$$

If only the light signal $E_1 \cos w_1 t$ were present, then

$$I_1 = (1/2)AE_1^2; \text{ smilarly } I_2 = (1/2)AE_2^2$$

Thus, the beat current output is

$$I_o = AE_1E_2 = 2(I_1I_2)^{1/2}$$

For large pump powers the beat signal current can be much larger than the current resulting if only the signal were present. The mean-square beat signal power resulting at the load resistor is:

$$S = (I_o^2/2)R_L = 2I_1I_2R_L$$

Thus the power gain comparing the cases of optical heterodyning and direct detection is:

$$G = (1/2I_o^2)/I_1^2 = 2I_2/I_1$$

For small signal powers this gain can be in the range of 10^5 to 10^6.

APPENDIX B

SIGNAL TO NOISE

The noise power output from a given pixel is due to optical shot noise, dark current shot noise, thermal noise of the load resistor, and referred noise to the input of the amplifier chain. The mean-square shot noise response of the pump signal must be modified from the normal shot noise expression to account for the photomixing operation. The pump shot noise term will be[1]:

$$I_{AS}^2 = 2qI_2(1+2n)B$$

where n is the quantum efficiency and B is the noise bandwidth.

A noise equivalent circuit for the optical heterodyning photodetector and amplifier circuit is shown in Figure 9. The equivalent noise current is

$$I_{eq}^2 = I_s^2 + I_L^2 + I_R^2 + \mathcal{L}_n^2 B/Z^2$$

where: I_s is the pump shot noise

I_L is the leakage current shot noise

I_R is the thermal noise of the load resistors

---

1. Van der Ziel, Noise in Measurement, Wiley, 1976 p. 189. Physica, 45. p. 379 - 1969.

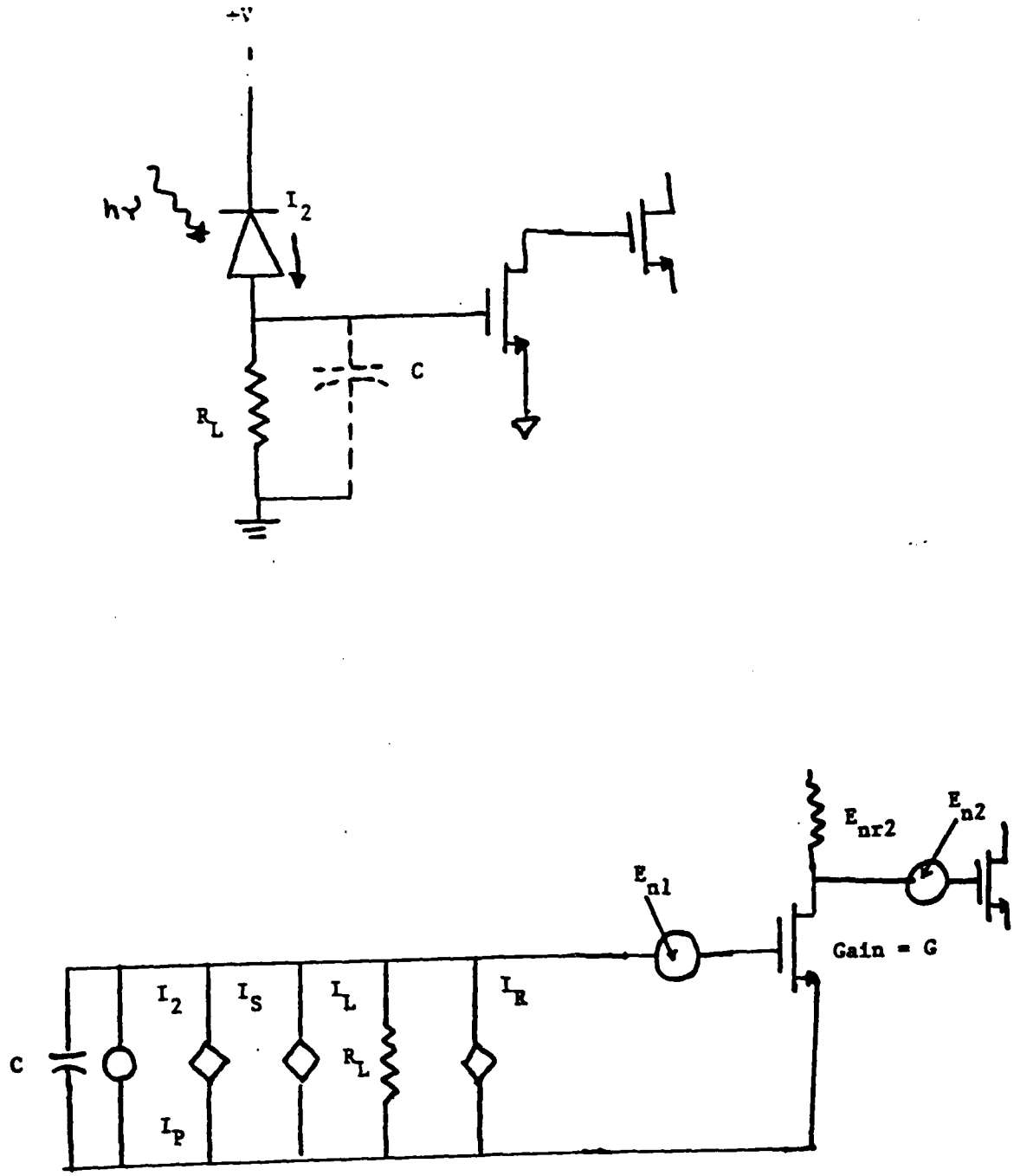

FIGURE 9 - NOISE EQUIVALENT CIRCUIT FOR THE OPTICAL HETERODYNE PHOTODETECTOR

E_n is the equivalent noise voltage of the MOSFET

Z is the input impedance

$Z = R_L \| (-jX_c)$

The 1/F term has been neglected because it will be removed by a bandpass filter following the amplifier.

Thus $I_{eq}^2 = 2qI_2(1+2n)B + 2qI_L B + 4kTB/R_L + En^2 B/R_L^2$

where

E_n is the equivalent input noise voltage of the amplifier.

The minimum detectable signal is calculated below. The signal to noise ratio is:

$$S/N = 1/2 I_o^2 R_L / I_{eq}^2 R_L$$

where I_o is the beat current output

$$I_o = AE_1E_2 = 2(I_1 \cdot I_2)^{1/2}$$

Thus,

$$S/N = 2I_1I_2 / 2qI_2(1+2n)B + 2qI_L B + 4kTB/R_L + E_n^2/R_L^2 \; B$$

APPENDIX C

The following two papers were presented at the 1982 SPIE meeting in San Diego.

-52-06

Optical excision in the frequency plane

Patrick J. Roth

Department of Defense
Fort George G. Meade, Maryland 20755

Abstract

This paper presents recent advancements in RF filtering techniques through the use of acousto-optics and a special purpose array of wideband photodiodes. An electronically programmable filter may be synthesized by inserting this array of photodiodes into the frequency plane of an optical spectrum analyzer. A description of the optical system, the photodiode array and some experimental results are presented.

Introduction

The reception and recording of wideband signals in various types of noise environments has been studied and analyzed for many decades. The enhancement of signal-to-noise ratios and improvement in the dynamic range for recording and communications purposes have incorporated such notch filter techniques as programmable digital filters, tunable L-C filters, and even superconducting filters for the excision of narrowband interference from the received information to be processed.

These electronic filter techniques are very effective in enhancing the signal-to-noise ratio of an RF signal. A source of error for these filters is the phase distortion which occurs at the bandstop-passband edges of the filter shape. These errors, although somewhat predictable, will add up and may severely distort the received signals when multiple filters are stacked in series.

Performing these RF filter functions in the frequency plane of an optical spectrum analyzer[1-4] has several advantages over the current electronic techniques. First, when some object is placed in the frequency plane of the optical spectrum analyzer, the magnitude of the affected frequency interval is attenuated and the phase remains constant. Also, the optical spectrum analyzer offers a high degree of parallelism which is a function of the time-bandwidth product associated with the acousto-optic cell chosen. Many filters may be realized simply by inserting more objects into the frequency plane. With the current technology, time-bandwidth products of 1000 are feasible with bandwidths ranging from 10 to 1000 MHz. This time-bandwidth product of 1000 implies 1000 resolvable frequency components.

Optical configuration

The optical excisor evaluated is shown in Figure 1. This configuration is a Mach-Zehnder interferometer[5] with an acousto-optic (AO) cell operating as a spectrum analyzer inserted in one path of the interferometer.

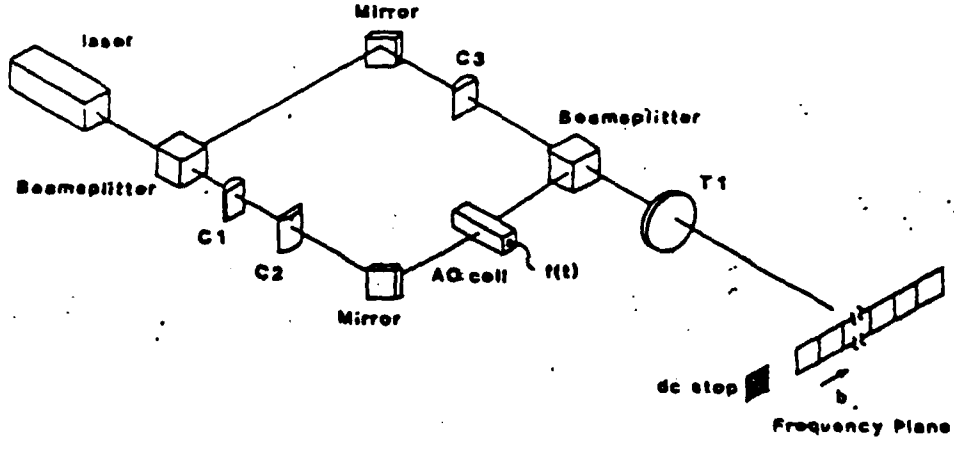

Figure 1. Interferometric spectrum analyzer

The cylinder lenses C1, C2 expand the laser beam to fill the aperture of the AO cell. Cylinder lens C3, in conjunction with the transform lens T1, expands the reference beam to illuminate the frequency plane with a flat reference wavefront. If this reference is not flat, some phase distortion may occur. For the same reason, the transform lens must be placed one focal length away from the frequency plane and one focal length away from the acousto-optic cell. The Excisor detector[6] is inserted into the frequency plane. This detector (Figure 2) consists of a linear array of 100 individual photodiodes whose photo-generated signals may be switched between one of two RF output summing busses. This switching capability is externally programmable. This detector architecture allows the summation of any combination of the 100 available contiguous frequency bands. All photo-signals not selected to appear on one summing bus will appear on the other summing bus.

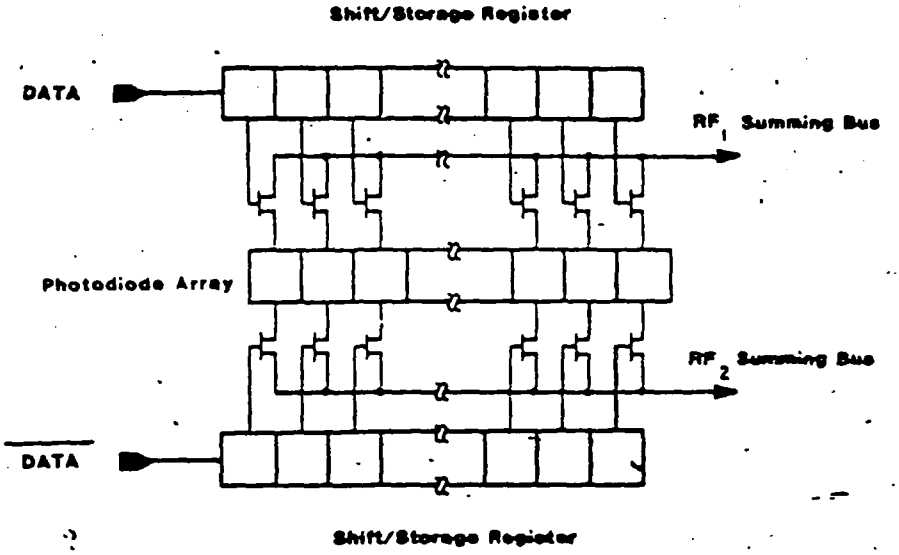

Figure 2. The Excisor detector

Theory

The collimated coherent input light is diffracted[7] through an angle proportional to the acoustic frequency present in the acousto-optic cell. This acoustic frequency results from the applied electrical signal f(t) (where f(t) is real). The acoustic wave propagates through the cell with velocity equal to v. The acoustic signal instantaneously contained within the cell may be represented as f(t-x/v), where x is the distance from the input transducer. The AO cell has a finite aperture equal to T, where T is the transit time of the acoustic wave in the AO cell. This finite aperture corresponds to an apodization of the acoustic signal such that the signal may now be represented by f(t - x/v - T/2). Also for this analysis, the AO cell is assumed to operate over an octave RF bandwidth (or less) and the positive diffraction order is used.

The optics takes the Fourier transform[8] of the acoustic signal with respect to the spatial variable x:

$$F(b,t) = \int_{-L/2}^{+L/2} f(t - \frac{x}{v} - \frac{T}{2})\, e^{-jbx}\, dx \qquad (1)$$

where L is equal to the length of the AO cell and b is the spatial frequency variable determined by the focal length of the transform lens and the relative acoustic velocity, v.

A change of variables (where $u = t - \frac{x}{v} - \frac{T}{2}$) yields:

$$F(b,t) = ve^{-j(t - \frac{T}{2})bv} \int_{t}^{t-T} f(u)\, e^{jbvu}\, du \qquad (2)$$

$$F(b,t) = ve^{-j(t - \frac{T}{2})bv} F^*(bv) \quad (3)$$

The exponential phase term indicates the light diffracted to position b is frequency shifted by an amount equal to the temporal frequency bv.

In addition to the transformed input signal, a reference wave is added into the frequency plane. The reference wave has a flat wavefront which may be parallel with the frequency plane or intersect the frequency plane at a small angle ϕ.

This reference wave with tilt angle ϕ may be written as $Ae^{j\phi b}$, where A is the amplitude of the reference wave. The total amplitude in the frequency plane is equal to the sum of the reference and the transform signal:

$$A_o(b,t) = Ae^{j\phi b} + ve^{-jbv(t - \frac{T}{2})} F^*(bv) \quad (4)$$

The corresponding intensity distribution is:

$$I_o(b,t) = |A_o(b,t)|^2 \quad (5)$$

The detector array is inserted into this frequency plane and since the detector array internally sums the outputs from each photodiode, this corresponds to an integration over the spatial variable b.

The output from the detector array with all outputs switched onto one summing bus is proportional to:

$$\int I_o(b,t)\, db = \int |A_o(b,t)|^2\, db \quad (6)$$

$$= \int |ve^{-jbv(t - \frac{T}{2})} F^*(bv) + Ae^{j\phi b}|^2\, db$$

$$= \int v^2F^2(bv)\, db + \int A^2\, db + 2\,Re \int AvF(bv)\, e^{jb(\phi + v(t - \frac{T}{2}))}\, db \quad (7)$$

The first two terms in Equation (7) do not contribute in band frequency components to the reconstruction of the original RF input signal. The last term after a change of variables (u = bv) becomes:

$$2\,Re\,A \int F(u)\, e^{ju(\frac{\phi}{v} + (t - \frac{T}{2}))}\, du = 2Af(t - \frac{T}{2} - \frac{\phi}{v}) \quad (8)$$

The last term of Equation (7) represents an inverse Fourier transform of the original Fourier transformed signal, which yields the original signal with a time delay equal to half the time aperture of the AO cell plus the delay corresponding to the tilt angle of the reference beam.

The detector allows the selection or rejection of any combination of frequency components by switching those components onto one of the two summing busses.

Test results

The AO cell in this system has a 20 MHz bandwidth centered at 45 MHz and an acoustic transit time of 50 microseconds.

The Excisor detector has 100 photodiode elements which correspond to a resolution bandwidth of 200 kHz.

The RF input to the AO cell is bandlimited Gaussian noise which demonstrates the filtering capabilities of this configuration. Figure 3 is the response to the Gaussian noise input. An HP scanning spectrum analyzer is the display device illustrating the various programmable filter functions. In Figures 3 through 7 and 10 through 15, the horizontal scale is 5 MHz per division, the vertical scale is 10 dB per division, and the IF resolution bandwidth is 100 kHz. Also, in Figures 3 through 15, the noise floor shown is the noise floor of the HP spectrum analyzer.

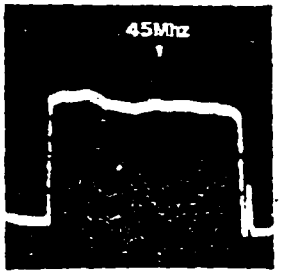

Figure 3. Response to bandlimited gaussian noise

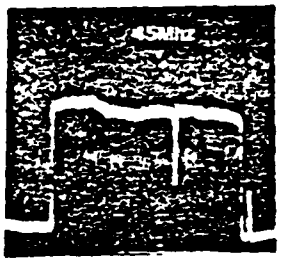

Figure 4. One diode switched - notch.

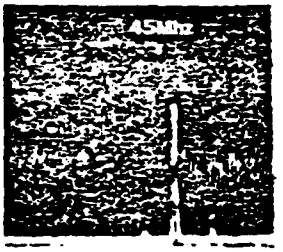

Figure 5. One diode switched - bandpass.

With all but one photodiode switched onto one of the summing busses, Figure 4 shows a 20 dB rejection in the Gaussian noise at a frequency corresponding to the selected photodiode. The other summing bus (Figure 5) simultaneously displays that portion of the Gaussian noise excised from Figure 4.

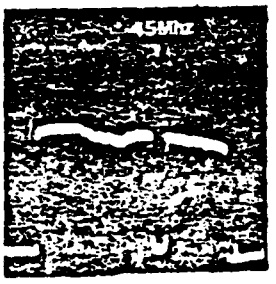

Figure 6. Three diodes switched - notch.

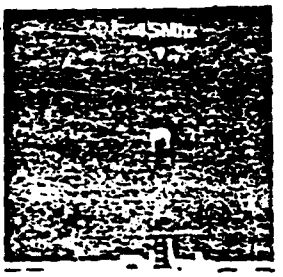

Figure 7. Three diodes switched - bandpass.

Figures 6 and 7 demonstrate the filtering capability when three adjacent photodiodes are switched to one of the summing busses. Figure 6 illustrates a notch depth of 30 dB. This difference is rejection (from Figure 4) may be attributed to crosstalk between adjacent photodiodes and the capacitance associated with the summing busses.

352-06

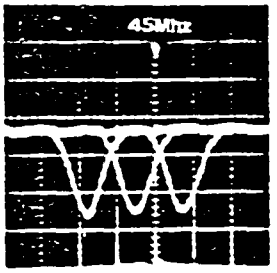

Figure 8. Notch response - superposition of three adjacent diodes.

Figure 9. Bandpass response - superposition of three adjacent diodes.

Figures 8 and 9 are a superposition of the frequency response from three adjacent photodiodes which illustrate the resolution of each photodiode. The horizontal scale is 200 kHz per division, the vertical scale is 10 dB per division, and the IF resolution bandwidth is 100 kHz.

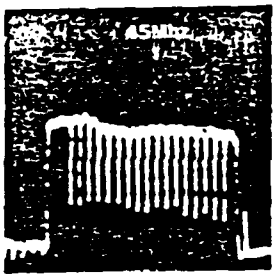

Figure 10. Comb notch filter.

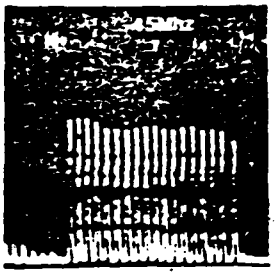

Figure 11. Comb ban pass filter.

Any combination of photodiodes may be switched between the two summing busses. With every fifth photodiode switched, Figures 10 and 11 illustrate a comb notch and comb bandpass filter. The horizontal scale is now 5 MHz per division, and the IF bandwidth is 100 kHz.

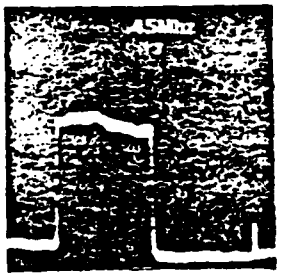

Figure 12. Low pass filter.

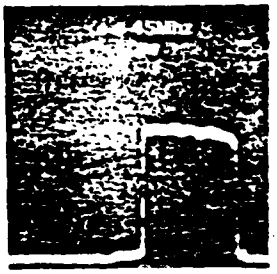

Figure 13. High pass filter.

With the first 50 elements switched to one summing bus and the remainder switched to the other summing bus, Figures 12 and 13 illustrate the synthesis of a low pass filter on one summing bus and a high pass filter on the other summing bus.

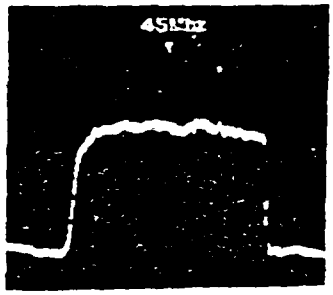

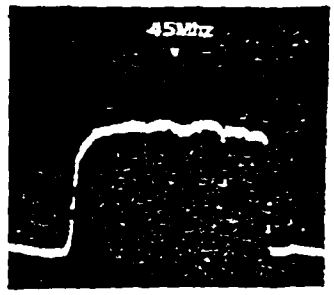

Figure 14. CW tone plus gaussian noise. Figure 15. CW tone excised from gaussian noise.

With the bandlimited Gaussian noise plus a CW tone 15 dB above the Gaussian noise input to the system (Figure 14), the photodiode corresponding to the CW tone is selected and switched off of the observed summing bus. Figure 15 illustrates the notch capability, which is 15 dB into the Gaussian noise signal.

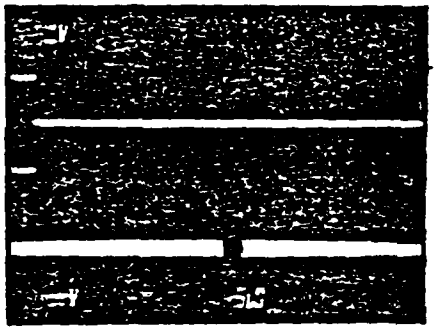

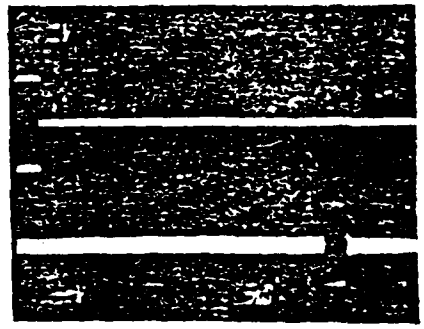

Figure 16. Reference wave untilted. Figure 17. Reference wave tilted.

Figure 16 illustrates the response of the system to a pulse which consists of a burst of the RF carrier at 45 MHz. This pulse input to the system demonstrates reconstruction at a time delay equal to one half the transit time of the AO cell (~25 microseconds) when the reference wave has a zero tilt angle. With the reference wave tilted, Figure 17 illustrates reconstruction at a time delay equal to 37.5 microseconds. The horizontal scale is 5 microseconds/division.

Conclusions

The detectors evaluated thus far have demonstrated a 3 dB bandwidth of 100 MHz (where each photodiode in the array has 100 MHz bandwidth). The maximum isolation observed between the summing busses, which is equivalent to notch depth for a single diode, has been 35 dB for a Gaussian noise input.

The laser used to evaluate the system is a 15 mW Helium Neon laser. This laser has proven to be insufficient to properly evaluate the dynamic range of the detector array. For optimum dynamic range, the RF drive to the acousto-optic cells should be at a minimum while the laser power should be at a maximum. To date, no saturation has been observed in the photodetector array or its associated output electronics. However, the signal-to-noise out for two CW tones input to the system was measured at 56 dB.

References

1. Hecht, D.L., "Spectrum Analysis Using Acousto-Optic Devices," SPIE Proceedings, Vol. 90, pp. 148-157. August 1976.
2. Bader, T.R., "Coherent Hybrid Optical Processors," SPIE Proceedings, Vol. 232. April 1980.

3. Bader, T.R., "Acousto-optic Spectrum Analysis: A High Performance Hybrid Technique," Applied Optics, Vol. 18, No. 10, pp. 1668-1672. 15 May 1979.
4. Turpin, T.M., "Spectrum Analysis Using Optical Processing," IEEE Proceedings, Vol. 69, No. 1, pp. 79-92. January 1981.
5. Vanderlugt, A., "Interferometric Spectrum Analyzer," Applied Optics, Vol. 20, No. 16, pp. 2270-2279. 15 August 1981.
6. Bluzer, Kub, and Borsuk, "Steering of High Frequency Low Level Photocurrents Between Summing Busses Beyond the gm/2πC Limit," I.E.D.M.. December 1980.
7. Hecht, D.L., "Multifrequency Acousto-optic Diffraction," IEEE Transaction on Sonics and Ultrasonics, Vol. SU-24, No. 1. January 1977.
8. Goodman, J.W., Introduction to Fourier Optics, New York, McGraw Hill, 1978.

Ignoring the first two terms as they are DC terms, dropping the scale factor of two, and setting $\omega=\omega$ yields:

$$\text{Detector Output} = \text{Re}\,[s(t-x)e^{j\omega t}] = s(t-x)\cos(\omega t) \quad (5)$$

which simply represents the original h(t) signal reproduced at each spatial position x with a time delay of x/v (v=1).

With each detector element reproducing one BPSK element, the BPSK elements can then be switched to one of the two summing busses. The BPSK elements are then integrated across the detector array onto the two summing busses, with the output dependent on the relative phases of the BPSK elements integrated together. With a specific mask pattern programmed into the detector switches, the outputs of the two summing busses are subtracted electrically, thereby producing the true correlation function between the detector mask pattern and the BPSK signal pattern, as follows:

Let: f(x) = detector mask pattern, where f(x) = 1 or -1 in desired correlation pattern. If f(x) = 1, the output of that detector is directed to the positive summing bus. If f(x) = -1, the output of that detector is directed to the summing bus which will be subtracted.

From (5), each detector output = s(t-x)cos(ωt), thus the total output g(t) is:

$$g(t) = \int[s(t-x)\cos(\omega t)]f(x)dx \quad (6)$$

$$g(t) = \cos(\omega t)\int s(t-x)f(x)dx \quad (7)$$

Equation (7) is simply the cos(ωt) carrier modulated by the convolution of the BPSK signal and the detector pattern. If the detector is programmed with the time reverse of the desired correlation pattern, i.e., the detector pattern = f(-x), the output becomes the correlation of s(t) and f(x) modulating the cos(ωt) carrier.

$$g(t) = \cos(\omega t)\int s(t-x)f(-x)dx \quad (8)$$

This correlator is exactly identical to a matched filter for the expected BPSK signal.

Experimental Implementation

The Excisor correlator as described was implemented using the architecture of Fig. 2. Fig. 3 is a photograph of the experimental set-up. In the actual implementation, the imaging lens system uses a standard 35 mm camera zoom lens. The zoom lens was chosen to allow for easy adjustment of the scaling of the BPSK keying elements in the Bragg cell to the detector element size. This is necessary as the scale factor will vary for different keying rates. The Bragg cell used was a 20 MHz, 50 us TeO_2 slow-shear wave device driven at approximately 150 milliwatts of RF power centered at 48 MHz. The two outputs of the detector busses were amplified by 55 dB and connected to two inputs of an oscilloscope vertical amplifier. The subtraction was accomplished by inverting one channel and adding the two channels. The correlator output is then displayed on the oscilloscope. Fig. 4 is a photograph of the oscilloscope display. The input signal for this output was the 48 MHz carrier being modulated by a 127 element long psuedo-random sequence clocked at 4 MHz. For this keying rate, the necessary scale factor for the imaging lens was approximately a five-to-one reduction. The detector was programmed with 100 consecutive elements of the 127 element long sequence. Computer simulation of this correlation showed that the ratio of the peak correlation value to the second-highest value should have been approximately 8.3. Examination of Fig. 4 shows that the experimental result is about 3.75. This rather poor agreement with the theoretical value can be attributed to the fact that the optical system was not optimal. The optical beam at the detector was not uniformly distributed and led to uneven contributions from the detector elements. The 3.75 ratio would indicate that only about half of the detector elements were actually contributing to the correlation value. However, Fig. 4 does show a definite correlation peak and was adequate to prove the feasibility of this correlator architecture. Optimization of the optical system should improve the results of the experiments and that remains to be done.

Summary

The feasibility of using the Excisor detector as a combination mask-photodetector has been demonstrated. The primary advantage of using this detector is its ability to be electronically programmed with static patterns. This feature makes it attractive for use in several signal processing applications.

352-07

OPTICAL CORRELATION USING THE EXCISOR DETECTOR

James L. Lafuse

Department of Defense
Ft. Meade, MD 20755

Abstract

Correlation of signals against a static mask is frequently used in signal processing. Many times it is useful to be able to rapidly change the mask. The programmable Excisor detector array can provide this capability when used as a combination mask and detector in an optical space integrating correlator. Such a correlator is described and experimental results are presented.

Introduction

Correlation of a signal against a fixed mask[1] is frequently used in signal processing to identify signal types and parameters. Many times the ability to frequently change the mask is desirable. The Excisor detector can provide this capability when used as both mask and detector in an optical space integrating correlator. The inherent electronic programming capability of the Excisor detector provides the flexibility required to make it useful in an operational system.

The Detector

The Excisor detector is a linear array of photodiode elements whose outputs can be individually switched to one of two current summing busses[2]. The photodiodes are switched by MOSFET switches located on both sides of the photodiodes. The gates of the switches are connected to the output of two parallel shift registers containing complementary data (Fig. 1). Thus, the diodes are switched by loading the appropriate data into the shift registers. The present design has a 100 element array with a bandwidth of 100 MHz and 35 dB of isolation between diodes. The center-to-center spacing of the diodes is 33 microns. This detector was originally developed to perform frequency Excision[3], hence, the name Excisor detector.

The Correlator

The correlator was implemented utilizing a Mach-Zender interferometer as shown in Fig. 2. The input signal, h(t), is assumed to be a bi-phase shift keyed (BPSK) RF signal of known and fixed keying rate. The Bragg cell is imaged onto the detector such that the image of one BPSK keying element is exactly the same length as the center-to-center spacing of the detector elements. As the detector is a square-law device, the mixing of the diffracted beam and reference beam, with the appropriate tilt, reproduces one keying element of the original h(t) in each detector element, as follows.

Let: $h(t)=s(t)\cos(\omega t)$

where s(t)=1 or -1 in any arbitrary pattern.

$$\text{Light Amplitude (diffracted)} = s(t-x/v)e^{j\omega(t-x/v)} \quad (1)$$

where x is the direction along the acoustic axis of the Bragg cell and v is the velocity of acoustic propagation in the Bragg cell. V will be assumed to be unity for simplicity.

The $e^{j\omega(t-x/v)}$ term is a doppler shift of the light arising from the moving signal in the Bragg cell. The $e^{j\omega}$ light term is assumed but not carried through.

Addition of the unity amplitude reference beam produces:

$$\text{Light Amplitude (combined)} = s(t-x)e^{j\omega(t-x)}+e^{j\alpha x} \quad (2)$$

where α is the angle of tilt between the undiffracted and reference beams.

Using the square law property of the detector:

$$\text{Detector Output} = |s(t-x)e^{j\omega(t-x)}+e^{j\alpha x}|^2 \quad (3)$$

$$\text{Detector Output} = s(t-x)^2+1+2\text{Re}\{s(t-x)e^{j[\omega t-(\omega-\alpha)x]}\} \quad (4)$$

352-U1

Acknowledgements

The author wishes to thank Douglas E. Brown for his generous help in reviewing the manuscript.

References

[1] Sprague, R., "A Review of Acoustic-Optic Signal Correlators," Proceedings SPIE., Vol. 90, pp. 136-147. August 1976.

[2] Borsuk, G., "Photodetectors for Acousto-Optic Signal Processors," Proceedings of the IEEE., Vol. 69, pp. 110-118. January 1981

[3] Roth, P., "Optical Excision in the Frequency Plane," To be published in this issue.

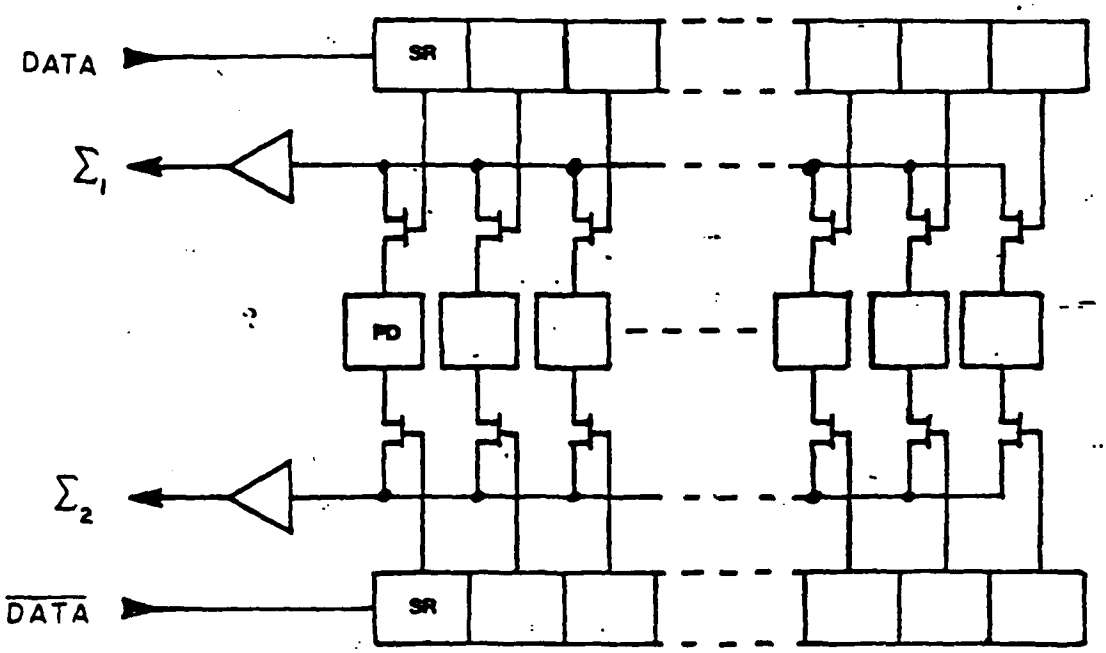

Figure 1. Programmable photodiode array.

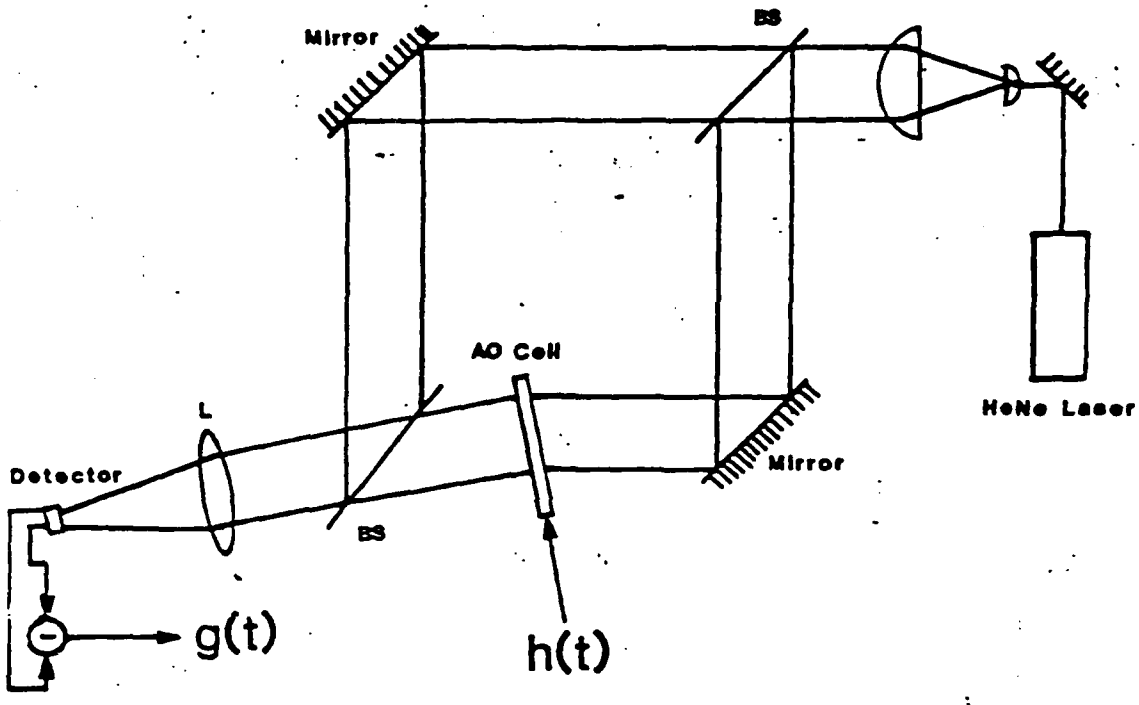

Figure 2. Simplified correlator architecture lens L represents an imaging lens system.

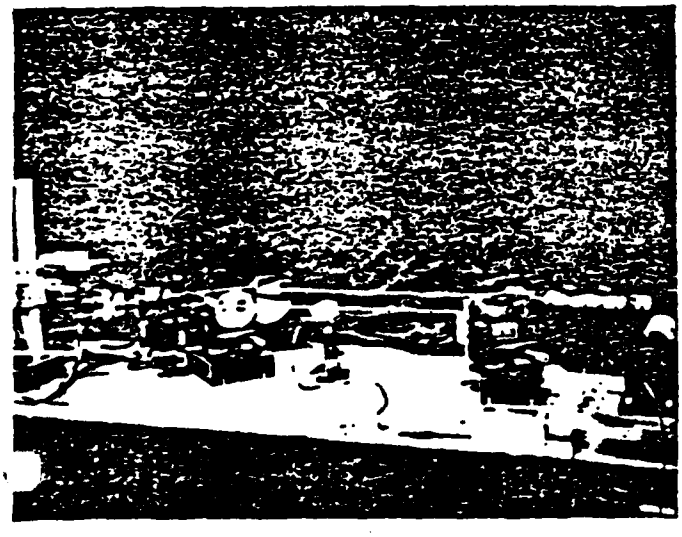

Figure 3. Experimental set-up.

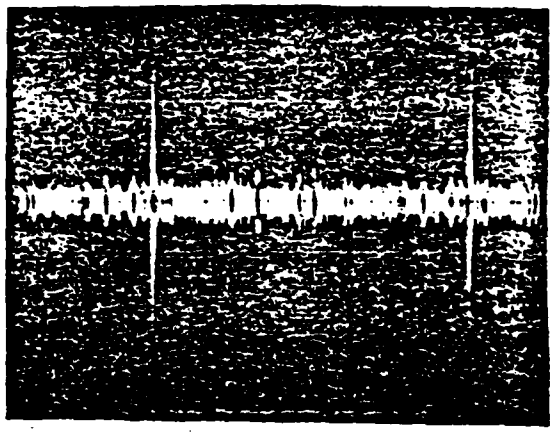

Figure 4. Oscilloscope display of correlator output.